Electronic supplementary information

Structural diversity directed by switchable coordination of substitute groups in a ternary Cu^{II}-triazole-sulfoisophthalate self-assembly system: Synthesis, crystal structures and magnetic behavior

En-Cui Yang,* Zhong-Yi Liu, Cui-Hua Zhang, You-Li Yang and Xiao-Jun Zhao*

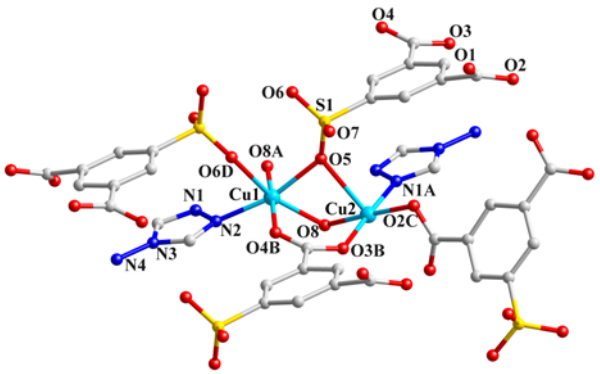

Fig. S1 Local coordination environments of Cu^{II} ions in **1** (H atoms were omitted for clarity, symmetry codes: A = – *x*, 1 – *y*, 2 – *z*; B = *x*, *y* – 1, *z*; C = – *x*, *y* – 0.5, 1.5 – *z*; D = 1 – *x*, 1 – *y*, 2 – *z*).

Table S1. Hydrogen-bonding parameters (Å, °) for **2**–**4**

D–H···A	*d* (D–H)	*d* (H···A)	*d* (D···A)	∠DHA
2				
O9–H9A··· O2 [a]	0.84	1.877	2.702	166.86
O9–H9B··· O7 [b]	0.84	1.977	2.716	146.14
O10–H10A···O6 [c]	0.84	1.907	2.720	162.65
O11–H11A··· O4 [c]	0.88	1.930	2.755	155.53
O12–H12B··· O11 [d]	0.84	2.208	2.998	155.67
3				
O(8)–H(8A)···O(2) [a]	0.85	1.857	2.704	174.82
N(4)–H(4")···O(5) [b]	0.90	2.294	3.175	166.49
N(4)–H(4') ···O(6) [c]	0.90	2.280	2.945	130.64
N(8)–H(8')···O(6) [d]	0.90	2.103	2.957	158.19
4				
N(8)–H(8A)···O(5) [a]	0.89	2.116	3.000	172.35
O(15)–H(15B)···O(9) [b]	0.85	2.001	2.754	147.02

Symmetry codes for **2**: [a] $1-x, 1-y, -z$; [b] $x-1, 1+y, z$; [c] $2-x, 1-y, -z$; [d] $x-1, y, z$. For **3**: [a] $1-x, 1-y, 1-z$; [b] $-x, -y, -z$; [c] $x-1, y-1, z$; [d] $x, y, z+1$. for **4**: [a] $1/2-x, y-1/2, z-1/2$; [b] $1/2-x, y+1/2, 1/2-z$.

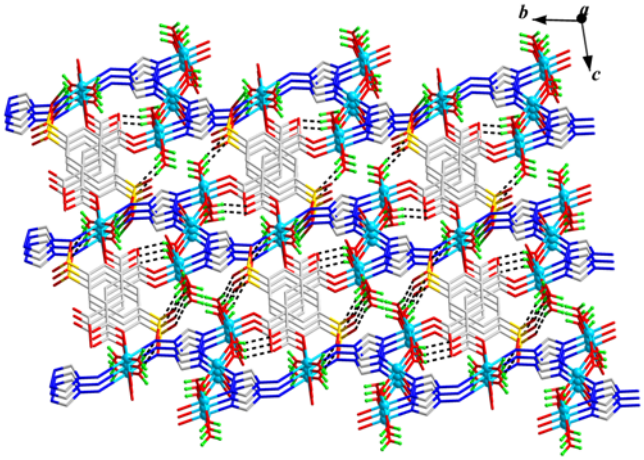

Fig. S2 3D supramolecular network of **2** by non-covalent O–H···O interactions.

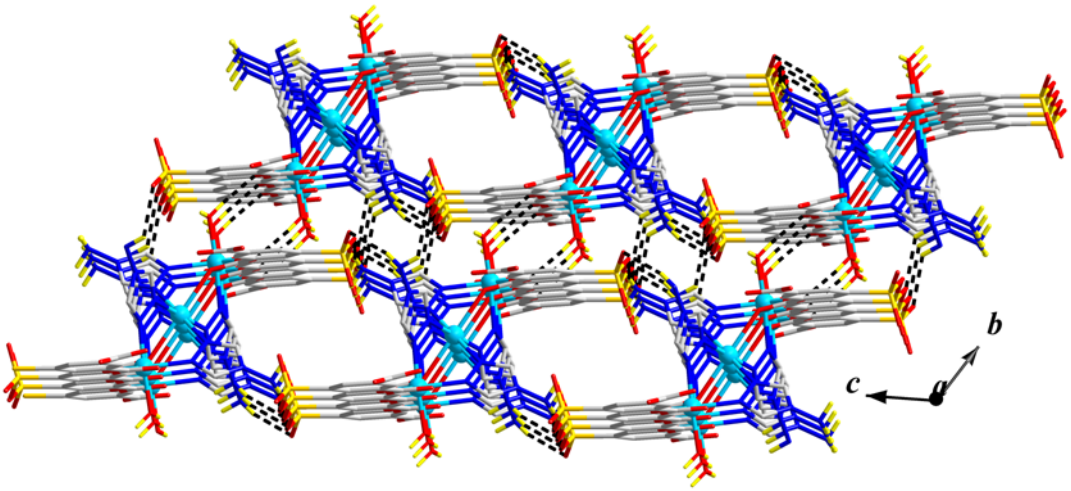

Fig. S3 3D supramolecular aggregate of **3** by inter-molecular O–H···O and N–H···O hydrogen-bonding interactions.

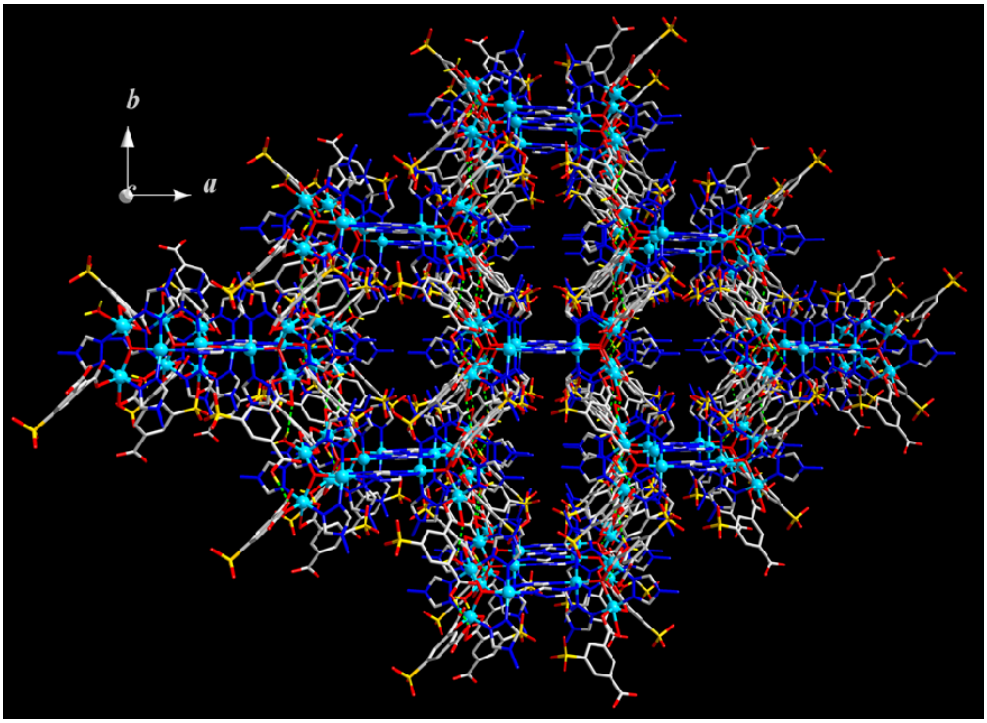

Fig. S4 3D supramolecular architecture of **4** by inter-molecular hydrogen-bonding interactions.

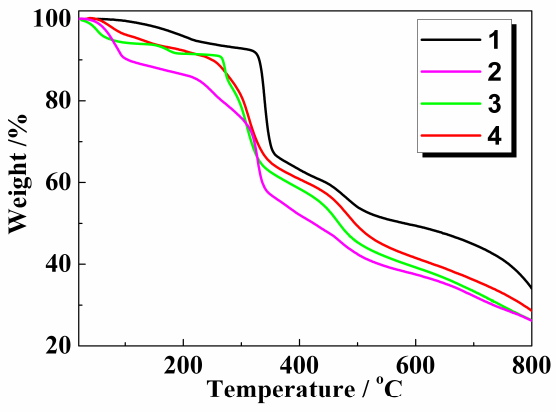

Fig. S5 TG curves for complexes **1–4**.

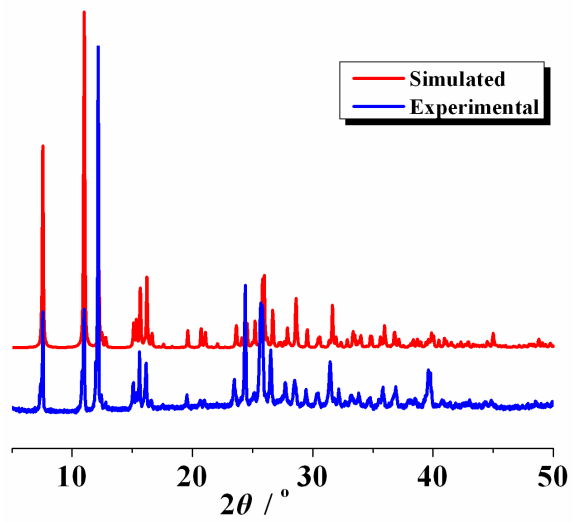

Fig. S6 Simulated (red) and experimental (blue) X-ray powder diffraction patterns for **1**.

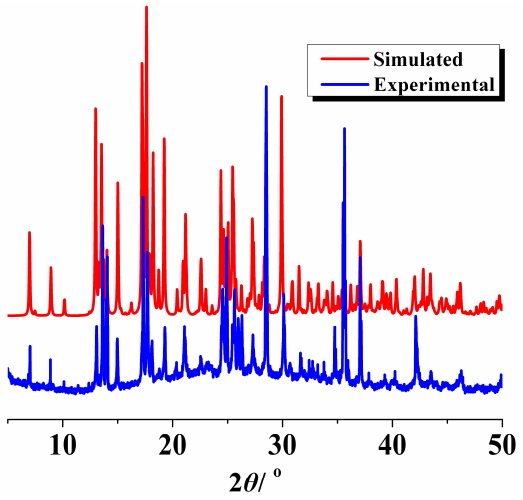

Fig. S7 Simulated (red) and experimental (blue) X-ray powder diffraction patterns for **2**.

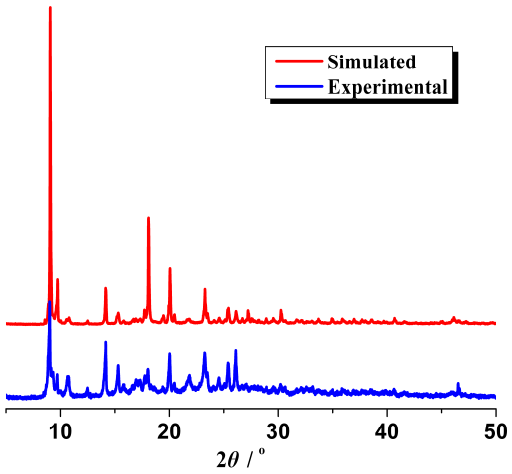

Fig. S8 Simulated (red) and experimental (blue) X-ray powder diffraction patterns for **3**.

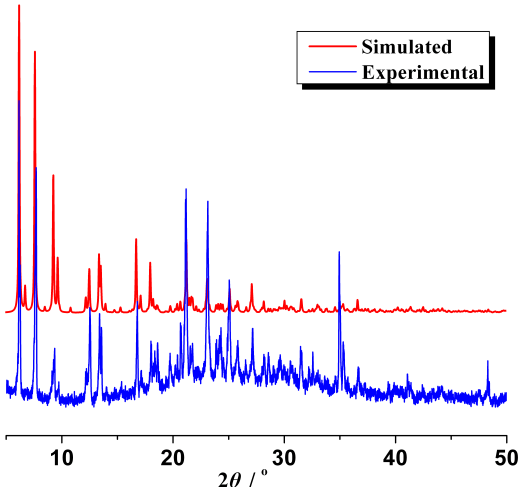

Fig. S9 Simulated (red) and experimental (blue) X-ray powder diffraction patterns for **4**.

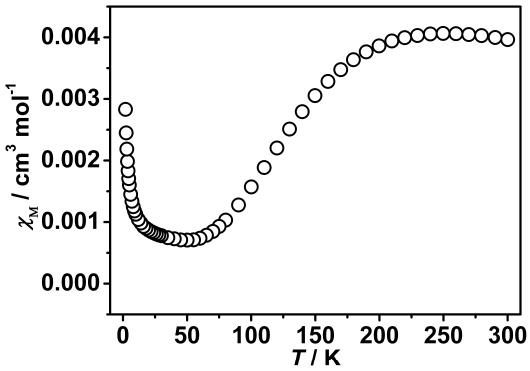

Fig. S10 Temperature dependence of χ_M for **1**.

Fitting equations for magnetic data

For **1**

$$\chi_M T = \chi_{Cu_4^{II}} T / [1-(zJ'\chi_{Cu_4^{II}} / Ng^2\beta^2)]$$

$$\chi_{Cu_4^{II}} = \frac{2Ng^2\beta^2}{kT}\left(\frac{A}{B}\right)$$

$$A = 5\exp(-E_1/kT) + \exp(-E_2/kT) + \exp(-E_3/kT) + \exp(-E_4/kT)$$

$$B = 5\exp(-E_1/kT) + 3\exp(-E_2/kT) + 3\exp(-E_3/kT) + 3\exp(-E_4/kT) + \exp(-E_5/kT) + \exp(-E_6/kT)$$

$$E_1 = -J_1 - J_2/2 - J_3$$

$$E_2 = J_1 - J_2/2 + J_3$$

$$E_3 = J_2/2 + [J_2^2 + (J_3 - J_1)^2]^{1/2}$$

$$E_4 = J_2/2 - [J_2^2 + (J_3 - J_1)^2]^{1/2}$$

$$E_5 = J_1 + J_3 + J_2/2 + [4(J_1^2 + J_3^2) + J_2^2 - 4J_1J_3 - 2J_2J_3 - 2J_1J_2]^{1/2}$$

$$E_6 = J_1 + J_3 + J_2/2 - [4(J_1^2 + J_3^2) + J_2^2 - 4J_1J_3 - 2J_2J_3 - 2J_1J_2]^{1/2}$$

For **2**

$$\chi_{Cu_3^{II}+Cu_1^{II}} = \frac{Ng^2\beta^2}{4kT}\left(\frac{1+e^{-2J/kT}+10e^{J/kT}}{1+e^{-2J/kT}+2e^{J/kT}}\right)+S(S+1)\frac{Ng^2\beta^2}{3kT}$$

$$\chi_M T = \chi_{Cu_3^{II}+Cu_1^{II}} T / [1-(zJ'\chi_{Cu_3^{II}+Cu_1^{II}} / Ng^2\beta^2)]$$

For **3**

$$\chi_{\text{linear } Cu_3^{II}} = \frac{Ng^2\beta^2}{4kT}\left(\frac{1+e^{-2J/kT}+10e^{J/kT}}{1+e^{-2J/kT}+2e^{J/kT}}\right)$$

$$\chi_M T = \chi_{Cu_3^{II}} T / [1-(zJ'\chi_{Cu_3^{II}} / Ng^2\beta^2)]$$

For **4**

$$\chi_{triangular\,Cu_3^{II}} = \frac{Ng^2\beta^2}{4kT}\left(\frac{1+5e^{3J/kT}}{1+e^{3J/kT}}\right)$$

$$\chi_M T = \chi_{Cu_3^{II}} T / [1-(zJ'\chi_{Cu_3^{II}} / Ng^2\beta^2)]$$